

# First Measurement of $R(X_{\tau/\ell})$ as an Inclusive Test of the $b \rightarrow c\tau\nu$ Anomaly

(The Belle II Collaboration)

## SUPPLEMENTAL MATERIAL

### Validation of the simulation reweighting

In Fig. 3 we illustrate the effect of the  $M_X$  and  $(p_\ell, M_X)$ -based reweightings of  $X\ell\nu$  and  $B\bar{B}$  background events on four key kinematic quantities, including the signal extraction quantities  $p_\ell^B$  and  $M_{\text{miss}}^2$ , the calibration quantity  $M_X$ , and a control quantity  $q^2 = ((\sqrt{s}, \vec{0}) - P_{B_{\text{tag}}}^* - P_X^*)^2$  that is used neither in the signal extraction nor in the reweighting. The reweightings improve the agreement between experimental and simulated data, best quantified by the normalized residuals, defined as the difference between simulated and experimental yields divided by the quadrature sum of their statistical uncertainties.

The reweightings have negligible effect on the  $p_\ell^B$  shape for  $B \rightarrow X_c\ell\nu$  events as the lepton momentum is largely independent of the hadronic  $X$  system. For  $B\bar{B}$  backgrounds, the lepton candidate's role in the  $B$ -meson decay chain is more complex, and the shape of the component is modified in the reweighting in the same-flavor control sample. This is reflected in modest improvements to the agreement in the low- $p_\ell^B$  region after the reweighting.

The remaining three quantities,  $M_X$ ,  $M_{\text{miss}}^2$ , and  $q^2$ , depend directly on the calibration quantity  $M_X$ . We observe large and simultaneous improvements in all of these quantities, seen in the figure as reduced residuals across all bins. The major improvements in  $M_{\text{miss}}^2$  and  $q^2$ , in particular, suggest that the reweightings mitigate the underlying modeling errors. The multiplicities of charged kaons, charged pions, and photons, not shown, also improve after reweighting. We tested the impact in various signal-depleted control regions in addition to the two mentioned: high- $M_X$  ( $M_X > 3 \text{ GeV}/c^2$ , 79% background and continuum events) and low- $M_{\text{miss}}^2$  ( $M_{\text{miss}}^2 < 1.5 \text{ GeV}^2/c^4$ , 78%  $B \rightarrow X\ell\nu$  events, 21% background and continuum events). We observe similar improvements, supporting the validity of the reweightings in all kinematic regions.

### Relationship between $R(X_{\tau/\ell})$ and $R(D^{(*)})$

In order to understand how the measured tau-to-light-lepton ratio of inclusive  $B$ -meson branching fractions  $R(X_{\tau/\ell})_{\text{exp}}$  relates to the  $R(D^{(*)})$  anomalies, it is essential to control for the variety of additional decays included in  $B \rightarrow X\tau(\ell)\nu$ . Aside from the  $D$  and  $D^*$  hadrons that are selected in the exclusive  $R(D^{(*)})$  mea-

surements, our events also contain  $D^{**}$ , nonresonant  $X_c$  ( $D_{\text{gap}}$ ), and minimal  $X_u$  contributions.

For this purpose, the measured light-lepton branching fractions  $\mathcal{B}(B \rightarrow D\ell\nu)$ ,  $\mathcal{B}(B \rightarrow D^*\ell\nu)$ , and  $\mathcal{B}(B \rightarrow X\ell\nu)$  are needed. For the inclusive branching fraction, we use the latest value from Ref. [45],

$$\mathcal{B}(B \rightarrow X\ell\nu) = (10.84 \pm 0.16)\%. \quad (1)$$

For the exclusive branching fractions, we calculate the isospin-averaged values of the  $B^+$  and  $B^0$  measurements summarized in the same reference, and use the arithmetic mean of the different  $B$ -meson lifetimes to obtain

$$\mathcal{B}(B \rightarrow D\ell\nu) = (2.27 \pm 0.06)\% \quad (2)$$

$$\mathcal{B}(B \rightarrow D^*\ell\nu) = (5.23 \pm 0.10)\%. \quad (3)$$

The standard model prediction of  $R(X_c)$  is calculated in Ref. [21], superseding Ref. [20], and in a different scheme in Ref. [22], while Refs. [21, 41] provide theoretical input for either fully inclusive  $R(X_{\tau/\ell})$  or  $R(X_u)$ . We average the predicted  $R(X_{\tau/\ell})$  value of Ref. [21] with a combination of  $R(X_c)$  and  $R(X_u)$  from Refs. [22, 41] using inclusive branching fractions from Ref. [45] to derive

$$R(X_{\tau/\ell})_{\text{SM}} = 0.223 \pm 0.005 \quad (4)$$

and accordingly

$$\mathcal{B}(B \rightarrow X\tau\nu) = (2.42 \pm 0.06)\%. \quad (5)$$

On its own,  $R(X_{\tau/\ell})_{\text{exp}}$  imposes an upper bound on the sum of measured  $R(D)$  and  $R(D^*)$  values,

$$\begin{aligned} R(X_{\tau/\ell})_{\text{exp}} \times \mathcal{B}(B \rightarrow X\ell\nu) &= \mathcal{B}(B \rightarrow X\tau\nu) \geq \\ &= \mathcal{B}(B \rightarrow D\tau\nu) + \mathcal{B}(B \rightarrow D^*\tau\nu) = \\ R(D) \times \mathcal{B}(B \rightarrow D\ell\nu) &+ R(D^*) \times \mathcal{B}(B \rightarrow D^*\ell\nu). \end{aligned} \quad (6)$$

By inserting the expected additional contributions to  $X\tau\nu$  we can write

$$\begin{aligned} \mathcal{B}(B \rightarrow X\tau\nu) &= \mathcal{B}(B \rightarrow D\tau\nu) + \mathcal{B}(B \rightarrow D^*\tau\nu) \\ &+ \mathcal{B}(B \rightarrow D_{(\text{gap})}^{**}/X_u\tau\nu). \end{aligned} \quad (7)$$

The size of these additional contributions can be calculated in the standard model by inserting predicted values for the semitauonic branching fractions based on measured light-lepton branching fractions,

$$\begin{aligned} \mathcal{B}(B \rightarrow D_{(\text{gap})}^{**}/X_u\tau\nu)_{\text{SM}} &= R(X_{\tau/\ell})_{\text{SM}} \times \mathcal{B}(B \rightarrow X\ell\nu) \\ &- R(D)_{\text{SM}} \times \mathcal{B}(B \rightarrow D\ell\nu) \\ &- R(D^*)_{\text{SM}} \times \mathcal{B}(B \rightarrow D^*\ell\nu) \\ &= (0.41 \pm 0.08)\%. \end{aligned} \quad (8)$$

This corresponds to  $(17.1 \pm 2.8)\%$  of the total semitauonic branching fraction given in Eq. (5). By assuming that all unmeasured additional semitauonic contributions are standard-model-like, we define the reduced ratio  $R(X_{\tau/\ell})^\dagger$  as

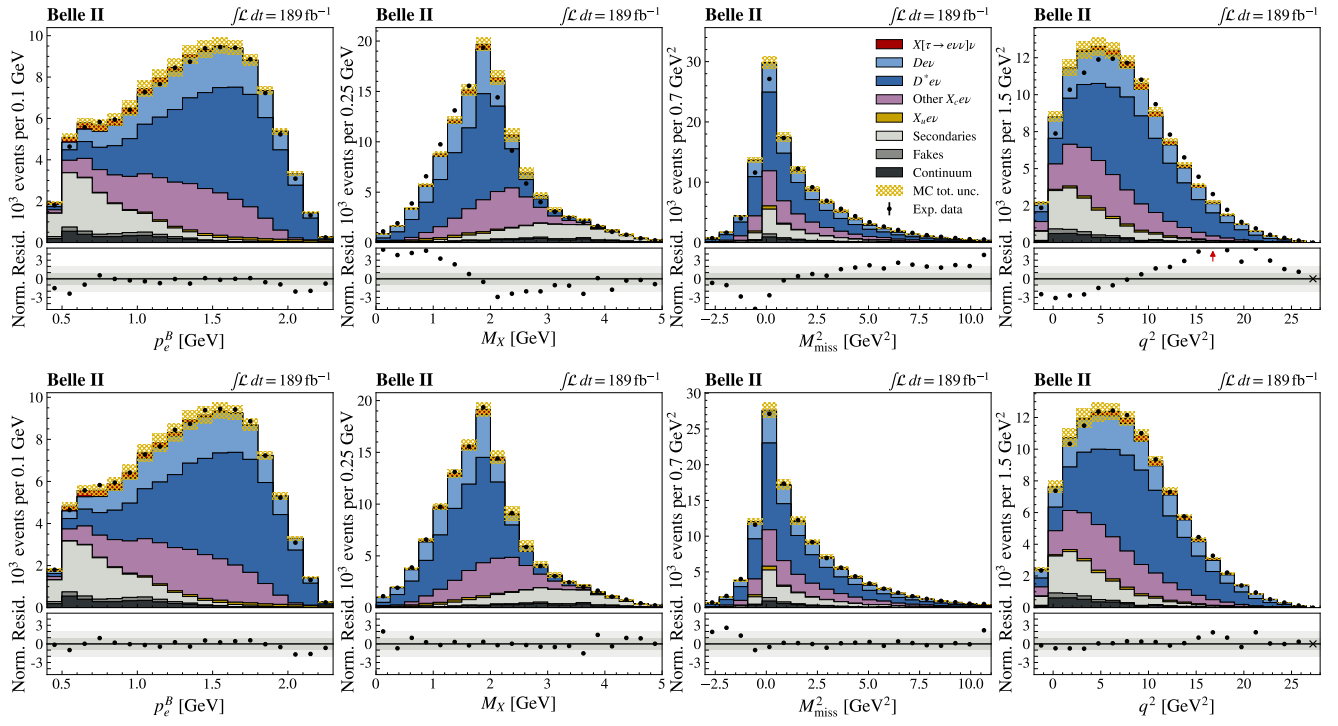
$$\begin{aligned} R(X_{\tau/\ell})^\dagger &\equiv \frac{\mathcal{B}(B \rightarrow X\tau\nu) - \mathcal{B}(B \rightarrow D_{(\text{gap})}^{**}/X_u\tau\nu)_{\text{SM}}}{\mathcal{B}(B \rightarrow X\ell\nu)} \\ &= R(X_{\tau/\ell})_{\text{exp}} - \frac{\mathcal{B}(B \rightarrow D_{(\text{gap})}^{**}/X_u\tau\nu)_{\text{SM}}}{\mathcal{B}(B \rightarrow X\ell\nu)} \end{aligned} \quad (9)$$

so that the full constraining power of  $R(X_{\tau/\ell})_{\text{exp}}$  on

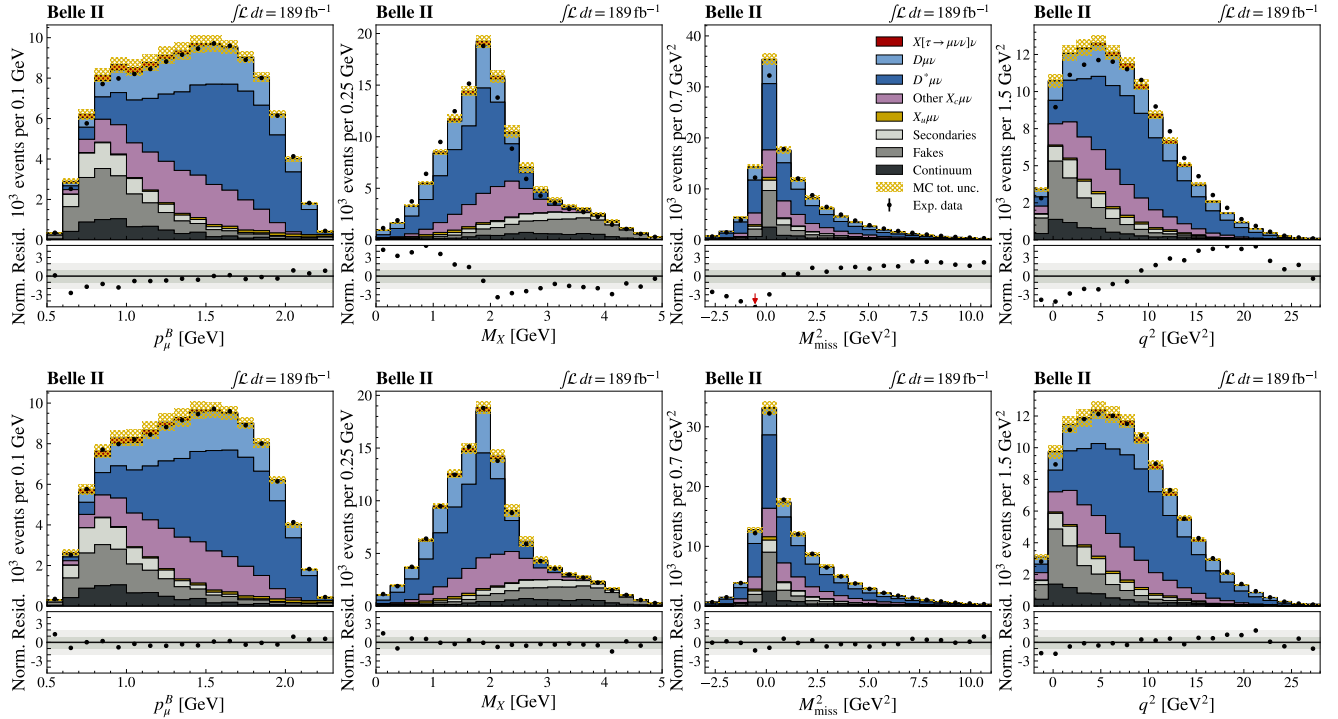
$R(D^{(*)})$  can be expressed as

$$R(X_{\tau/\ell})^\dagger \times \mathcal{B}(B \rightarrow X\ell\nu) = x_{R(D)} \times \mathcal{B}(B \rightarrow D\ell\nu) + y_{R(D^*)} \times \mathcal{B}(B \rightarrow D^*\ell\nu). \quad (10)$$

Here, we have replaced the experimental value of  $R(D)$  ( $R(D^*)$ ) by the running quantity  $x_{R(D)}$  ( $y_{R(D^*)}$ ) so that these findings can directly be summarized in the  $R(D) - R(D^*)$  plane that compares measured and predicted  $R(D^{(*)})$  values. Solving Eq. (10) for  $y_{R(D^*)}$  converts the measured  $R(X_{\tau/\ell})$  value into a straight line on the plane as depicted in Fig. 2.



(a) Electron channel before (top) and after (bottom) the simulation reweighting.



(b) Muon channel before (top) and after (bottom) the simulation reweighting.

Figure 3: The effect of the  $M_X$  and  $(p_\ell - M_X)$ -based reweighting on four key kinematic quantities for the electron (a, top) and muon (b, bottom) channels. The top rows show the pre-reweighting distributions in simulated (filled histograms) and experimental (black points) data, with their uncertainty-normalized disagreement (“Norm. Resid.”) shown below. The bottom row of plots shows the reweighted distributions, with significantly reduced residuals.